Numerical investigation of multiphase flow in a channel

Uktam Salomov[1*], *Murodil* Madaliyev[1], and *Akmaljon* Kuchkarov[1]

[1]Fergana Polytechnic Institute, 150107 Fergana, Uzbekistan

Abstract. Due to the occurrence of failures are divided into design, production and operational. Structural failures occur due to imperfection or violation of the established rules and (or) norms for the design of an object. Production - arise as a result of improper assignment of technological processes for the manufacture or restoration of parts and assembly of a car or are the result of a violation of the accepted technology, unsatisfactory quality of the material of parts or coatings applied to them, the use of insufficiently accurate measuring instruments, failure to meet technical requirements for the manufacture and assembly of elements, as well as the manufacture and assembly of elements and the object as a whole. In the article, basic information about the principles of calculations for solving a system of multiphase Navier–Stokes equations using the control volume method is provided. It is shown that the relationship between velocities and pressure is found using the procedure of SIMPLE. For the numerical solution of this problem, the McCormack scheme was applied. A comparison has been made between each other and with the experimental data. For turbulence, the Spalart–Allmares model was used. And also in the work the movement of sedimentary fluid in different diameters and different Reynolds numbers was studied.

1 Introduction

As one of the ways to obtain new knowledge, mathematical modeling is one of the main research methods in various fields of natural science today. The movement of gas in a wind tunnel, the propagation of tsunami waves, the spread of plasma in a trap, weather changes and other numerous phenomena in science and technology are described by various mathematical models represented as integral or partial differential equations. Modern computational algorithms make it possible to solve these systems of equations with sufficient accuracy in two-dimensional and three-dimensional approximations when solving various classes of problems, taking into account real geometries and non-stationarity of the process. Further progress in the development of numerical methods is associated with the development of new numerical algorithms and an increase in the speed and power of modern computer technology [1]. Modern numerical methods speed up the process of developing new products, allow you to point out the weaknesses of existing ones, but the question arises about the reliability of the results obtained. The accuracy of the results obtained using these

* Corresponding author: ims-79@mail.ru

calculations depends on the choice of turbulence models, as well as on the number of elements of the computational grid [2].

2 Physical and mathematical statement of the problem

A two-dimensional turbulent flow in a flat channel is considered. The physical picture of the analyzed flow and the configuration of the computational domain are shown in Figure1. Here, the height of the channel is H=1 cm, the length of the channel is L=57 cm.

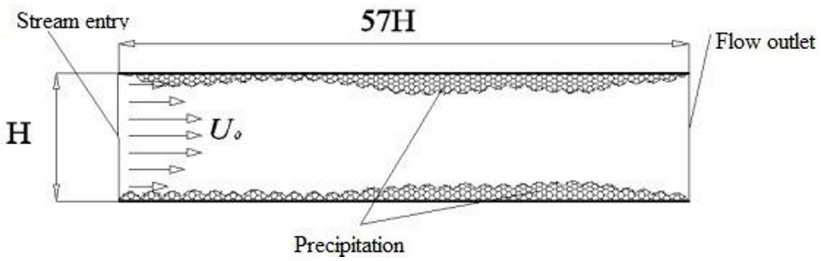

Fig. 1. Scheme of the computational domain in a flat channel.

At the entrance to the channel in the section, the flow profile was set for the longitudinal velocity -U/U0=1 and the transverse velocity -V and pressure -p equal to zero. When dimensionless values are introduced, the channel height -H is taken as the length scale, and the average flow rate - at the channel inlet is taken as the velocity scale. For the numerical study of the problem posed, the system of Navier-Stokes equations averaged over Reynolds is used, taking into account the interaction between the phases [3]. The system of equations does not take into account the forces due to the effects of turbulent migration, Sefman, Magnus (lift force) and Coriolis [4]. Because they are significantly less than the force of gravity. Thus, for mathematical modeling of the processes of transfer of dust particles and aerosols in a channel, it is sufficient to take into account the gravity force and the Stokes force of interaction between the phases [5].

$$\begin{cases} \dfrac{\partial \bar{U}_j}{\partial x_j} = 0, \\ \dfrac{\partial \bar{U}_i}{\partial t} + \bar{U}_j \dfrac{\partial \bar{U}_i}{\partial x_j} = -\dfrac{1}{\rho}\dfrac{\partial p}{\partial x_i} + \dfrac{\partial}{\partial x_j}\left[\nu \left(\dfrac{\partial \bar{U}_i}{\partial x_j} + \dfrac{\partial \bar{U}_j}{\partial x_i} \right) \right] + \dfrac{1}{\rho}\dfrac{\partial}{\partial x_j}\left(-\rho \overline{u'_i u'_j} \right) - \sum_{m=1}^{N} \dfrac{\rho_m}{\rho} k_m \left(\bar{U}_i - \bar{U}p_i \right), \\ \dfrac{\partial \bar{U}p_i}{\partial t} + \bar{U}_j \dfrac{\partial \bar{U}p_i}{\partial x_j} = k_m \left(\bar{U}_i - \bar{U}p_i \right), \\ \dfrac{\partial \rho_m}{\partial t} + \bar{U}p_j \dfrac{\partial \rho_m}{\partial x_j} = D \dfrac{\partial}{\partial x_j}\left[\dfrac{\partial \rho_m}{\partial x_j} + \dfrac{\partial \rho_m}{\partial x_i} \right]. \end{cases} \quad (1)$$

here $\bar{U}_i$ – is the axial, radial and tangential components of the air flow velocity, respectively; $\bar{U}p_i$ - similar velocity components for the m-th fraction of sedimentary substances; $\bar{p}$ – hydrostatic pressure; ρ – gas density; ν - its molecular viscosity; $\rho\overline{u'_i u'_j}$

- components of the Reynolds stress tensor; ρ_m - mass density of sedimentary substances; k_m - coefficient of interaction between air and the m-th fraction of sedimentary substances; N- number of fractions of sedimentary substances; $D = \frac{\rho}{S_c(\rho+\rho_\rho)}\left(\nu + \left(-\overline{u'v'}\left(\frac{\partial \overline{U}_i}{\partial x_j}\right)^{-1}\right)\right)$ - diffusion coefficient for the sedimentary phase, $Sc = 0.8$ - Schmidt coefficient. The paper considers the number of fractions N=4.

The interaction coefficient between the phases was determined through the Stokes parameter:

$$k_m = \frac{18\rho\nu}{\rho_\rho \delta_m^2}.$$

In this expression ρ_ρ - sediment density, δ_m - "effective" sediment diameter.

The system of Navier-Stokes equations averaged over Reynolds (1) is not closed. To close this system in linear models, the generalized Boussinesq hypothesis is used.

$$-\overline{u_i' u_j'} = \nu_t\left(\frac{\partial \overline{U}_i}{\partial x_j} + \frac{\partial \overline{U}_j}{\partial x_i}\right) - \frac{2}{3}k\delta_{ij}. \tag{2}$$

Here ν_t - turbulent viscosity.

3 Spalart-allmares model

To find the turbulent viscosity, the Spalart-Allmares SA turbulence model was used in the work. The SA model [6] belongs to the class of one-parameter turbulence models. Here there is only one additional equation for calculating the kinematic coefficient of eddy viscosity

$$\frac{\partial \tilde{\nu}}{\partial t} + \overline{U}_j \frac{\partial \tilde{\nu}}{\partial x_j} = C_{b1} f_{r1} \tilde{S}\tilde{\nu} - C_{w1} f_w \left(\frac{\tilde{\nu}}{d}\right)^2 + \frac{1}{\sigma_\nu}\left[\frac{\partial}{\partial x_j}\left((\nu+\tilde{\nu})\frac{\partial \tilde{\nu}}{\partial x_j}\right) + C_{b2}\frac{\partial \tilde{\nu}}{\partial x_i}\frac{\partial \tilde{\nu}}{\partial x_i}\right]. \tag{3}$$

Turbulent eddy viscosity is calculated by the formula: $\nu_t = \tilde{\nu} f_{v1}$

The function f_{r1} is a correction factor that describes the effect of streamline curvature on turbulence. This function has the following form:

$$f_{r1} = (1+C_{r1})\frac{2r^*}{1+r^*}\left[1 - C_{r3}\tan^{-1}(C_{r2}\hat{r})\right] - C_{r1},\ \hat{r} = \frac{2\Omega_{i,k}S_{j,k}}{D^4}\left(\frac{DS_{i,j}}{Dt}\right),\ D^2 = \frac{1}{2}\left(S^2+\Omega^2\right),$$
$$\frac{DS_{i,j}}{Dt} = \frac{\partial S_{ij}}{\partial t} + u_k\frac{\partial S_{ij}}{\partial x_k},\ S_{i,j} = \frac{1}{2}\left(\frac{\partial u_i}{\partial x_j} - \frac{\partial u_j}{\partial x_i}\right),\ \Omega_{i,j} = \frac{1}{2}\left[\left(\frac{\partial u_i}{\partial x_j} - \frac{\partial u_j}{\partial x_i}\right)\right],\ S^2 = 2S_{ij}S_{ij},$$
$$\Omega^2 = 2\Omega_{ij}\Omega_{ij},\ r^* = S/\omega,\ C_{r1} = 1,\ C_{r2} = 12,\ C_{r3} = 1. \tag{4}$$

where S_{ij} — strain rate tensor, DS_{ij}/Dt — components of the substantial derivative of the strain rate tensor, Ω_{ij} — тензор завихренности. The remaining values remain the same

as for the "standard" model, which are presented in [7]. Obvious no-slip boundary conditions are set on all fixed solid walls $U\big|_{\Gamma}=V\big|_{\Gamma}=\tilde{v}\big|_{\Gamma}=0$, where Γ – hard boundary [8].

4 The method of solution

For the numerical solution of the system of initial non-stationary equations (1) for the scheme, the method of finite differences was used. Due to the complexity of matching the velocity and pressure fields for discretization of the equations of motion in X,Y directions and the continuity equation, a grid with a spaced arrangement of grid nodes for dependent variables was used. This means that the velocity and pressure components are determined at different nodes. This approach is similar to the SIMPLE methods and provides certain advantages in calculating the pressure field [9]. The arrangement of cells and nodes is similar to that of the SIMPLE method.

5 The scheme of McCormack

In computational hydrodynamics, the McCormack method is a widely used discretization scheme for the numerical solution of hyperbolic partial differential equations. This second-order finite difference method was introduced by Robert W. McCormack in 1969 [10]. McCormack's method is elegant, easy to understand and easy to program. The McCormack method is widely used to solve the equations of hydrodynamics. McCormack is especially useful for solving non-linear partial differential equations such as the Euler and Navier-Stokes equations. The system of equations (1) can be represented in matrix form.

$$\frac{\partial \Phi}{\partial t}+\frac{\partial U\Phi}{\partial x}+\frac{\partial V\Phi}{\partial y}=\frac{\mu}{\rho}\left(\frac{\partial^2\Phi}{\partial x^2}+\frac{\partial^2\Phi}{\partial y^2}\right)+\Pi^{\Phi}. \tag{5}$$

Applying the explicit predictor-corrector method to the nonlinear Navier-Stokes and SA equations, we obtain the following difference scheme:

Predicator

$$\bar{\Phi}_{i,j}=\Phi^n_{i,j}-\Delta t(U^n_{i,j}\frac{\Phi^n_{i+1,j}-\Phi^n_{i,j}}{\Delta x}+V^n_{i,j}\frac{\Phi^n_{i,j+1}-\Phi^n_{i,j}}{\Delta y})+\Delta t(\frac{\Phi^n_{i,j+1}-2\Phi^n_{i,j}+\Phi^n_{i,j-1}}{\mathrm{Re}\,\Delta y^2}+\frac{\Phi^n_{i+1,j}-2\Phi^n_{i,j}+\Phi^n_{i-1,j}}{\mathrm{Re}\,\Delta x^2}+\Pi^{\Phi}). \tag{6}$$

Corrector

$$\Phi^{n+1}_{i,j}=\frac{1}{2}\left(\begin{array}{l}\bar{\Phi}_{i,j}+\Phi^n_{i,j}-\Delta t(\bar{U}^n_{i,j}\frac{\bar{\Phi}^n_{i,j}-\bar{\Phi}^n_{i-1,j}}{\Delta x}+\bar{V}^n_{i,j}\frac{\bar{\Phi}^n_{i,j}-\bar{\Phi}^n_{i,j-1}}{\Delta y})+\\ +\Delta t(\frac{\bar{\Phi}_{i,j+1}-2\bar{\Phi}_{i,j}+\bar{\Phi}_{i,j-1}}{\mathrm{Re}\,\Delta y^2}+\frac{\bar{\Phi}_{i+1,j}-2\bar{\Phi}_{i,j}+\bar{\Phi}_{i-1,j}}{\mathrm{Re}\,\Delta x^2}+\Pi^{\Phi})\end{array}\right). \tag{7}$$

Here

$$\Phi = \begin{pmatrix} U \\ V \\ \tilde{v} \end{pmatrix}, \quad \Pi^{\Phi} = \begin{pmatrix} \dfrac{\partial p}{\rho \partial x} \\ \dfrac{\partial p}{\rho \partial y} \\ C_{b1}\left(1-f_{t2}\right)\tilde{S}\tilde{v} - \left[C_{w1}f_w - \dfrac{C_{b1}}{k^2}f_{t2}\right]\left(\dfrac{\tilde{v}}{d}\right)^2 + \dfrac{C_{b2}}{\sigma}\left(\left(\dfrac{\partial \tilde{v}}{\partial x}\right)^2 + \left(\dfrac{\partial \tilde{v}}{\partial y}\right)^2\right) \end{pmatrix}.$$

This is an explicit scheme of the second order of accuracy in time and space with an approximation error $O\left((\Delta t)^2, (\Delta x)^2, (\Delta y)^2\right)$, this scheme is stable at $\left(\dfrac{U_{\max}\Delta t}{\Delta x} + \dfrac{V_{\max}\Delta t}{\Delta y}\right) \le 1$.

Initially (predictor) is an estimate $\overline{\Phi_i^{n+1}}$ values and at $n+1$-м time step, and then (corrector) the final value is determined Φ_i^{n+1} at $n+1$-st time step. Note that in the predictor it is approximated by forward differences, and in the corrector, by backward differences.

6 Calculation grids

In computational fluid dynamics, it is extremely important that the simulation correctly represents the conceptual model. Moreover, the simulation should resemble real flows as closely as possible. Numerical simulation has various advantages over experiments [2]. The main one is that the parameters can be easily changed and quick results are possible at a lower cost. In this study, a computational grid was used, which is refined near the channel walls Figure. 2.

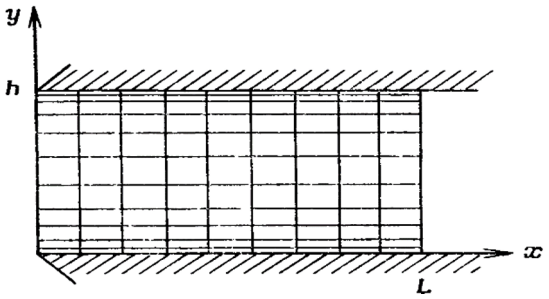

Fig. 2. Refining the mesh near the channel wall

Grinding is carried out using the following formula

$$y = h\frac{(\beta+2\alpha)\left[(\beta+1)/(\beta-1)\right]^{(\bar{y}-\alpha)/(1-\alpha)} - \beta + 2\alpha}{(2\alpha+1)\left\{1+\left[(\beta+1)/(\beta-1)\right]^{(\bar{y}-\alpha)/(1-\alpha)}\right\}}. \tag{8}$$

If $\alpha = 0$, then the grid will be refined only near $y = h$, while if $\alpha = 1/2$, then the grid will be refined as near $y = 0$ so around $y = h$. Roberts showed [2, 13] that the stretching parameter β is approximately related to the dimensionless thickness of the boundary layer δ / h in the following way:

$\beta = (1-\delta/h)^{-1/2}$, $0 < \delta/h < 1$.

where h — grid size in direction y. For the first case used, grid number is 1000×100.

7 Calculation results and their discussion

Figure 3 shows the results of the longitudinal velocity in various sections along the length of the channel. Reynolds number Re=27000.

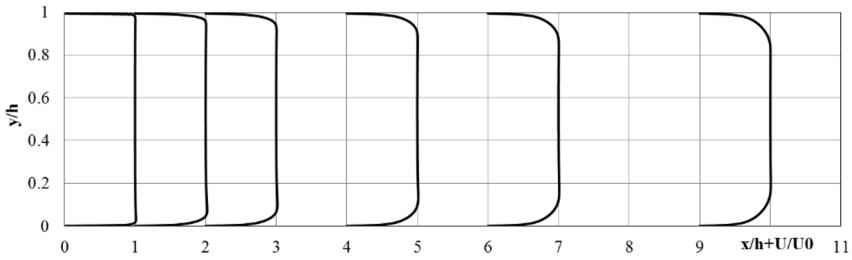

Fig. 3. Longitudinal velocity in various sections along the length of the channel.

U_0– is the reference velocity in the center channel used for the dimensionless determination of velocity profiles [11].

Figure 4 shows the results of the transverse velocity in various sections along the length of the channel. Reynolds number Re=27000.

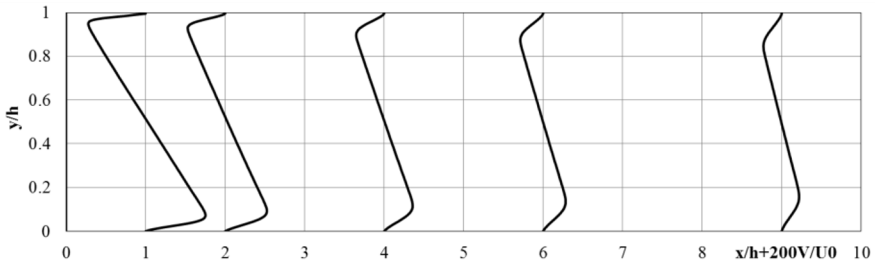

Fig. 4. Transverse velocity in various sections along the length of the channel.

Now we compare the numerical results with the experimental data in Fig.5. Reynolds number Re=27000.

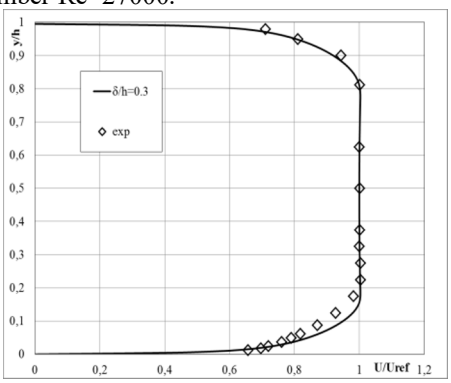

a

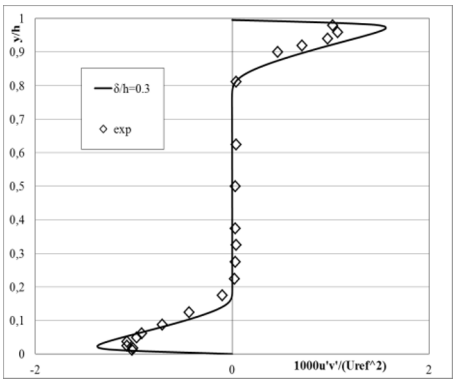

b

Fig. 5. Comparison of numerical results with experimental data a) longitudinal flow velocity, b) Reynolds stresses.

Here U_{ref}– is the reference speed in the center channel.

Comparisons of the obtained numerical results with known experimental data are shown below. On figure. 6 shows the numerical results of changing the Reynolds number of the momentum loss thickness from the dimensionless plate length x. The Reynolds number of momentum loss thickness was found by integrating the equation

$$\frac{d\,\mathrm{Re}_\theta}{dx} = 0.5C_f. \tag{9}$$

Here C_f - plate friction coefficient:

$$C_f = \frac{2}{\mathrm{Re}}\left(\frac{\partial V_x}{\partial y}\right). \tag{10}$$

Figure 6 shows the experimental results for comparison

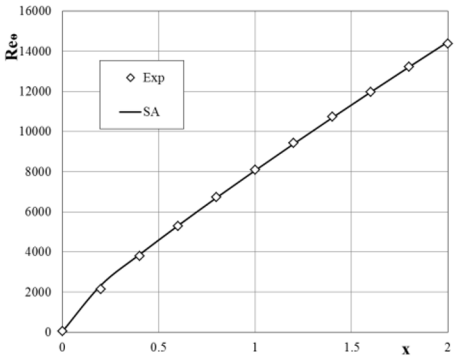

Fig. 6. Dependence of the Reynolds number of the momentum loss thickness on the length of the plate.

In Figure 7, the solid line shows the dependence of the friction coefficient on the dimensionless momentum loss thickness according to the proposed model. Diamonds are also illustrated by results on the Karman-Schoencher theory [12].

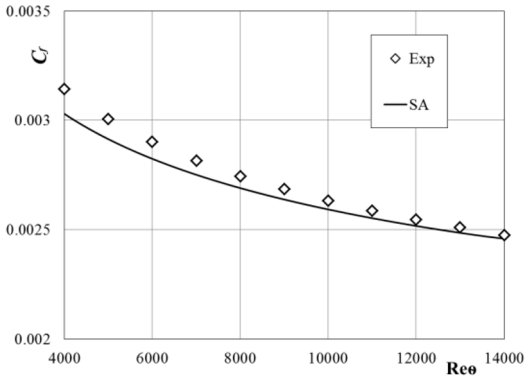

Fig. 7. Dependence of the coefficient of friction on the Reynolds number of the momentum loss thickness.

The solid line in Figure 8 shows the result of numerical calculation for the dimensionless longitudinal flow velocity depending on the dimensionless distance to the plate. Dimensionless velocities and distance were determined by the formulas

$$u^+ = \frac{V_x}{u^*}, \quad y^+ = \mathrm{Re}\, y u^*, \; u^* = \sqrt{0.5 C_f}. \tag{11}$$

Here, for comparison with the results of the diamond model, the results of the Coles theory are also shown [13,14].

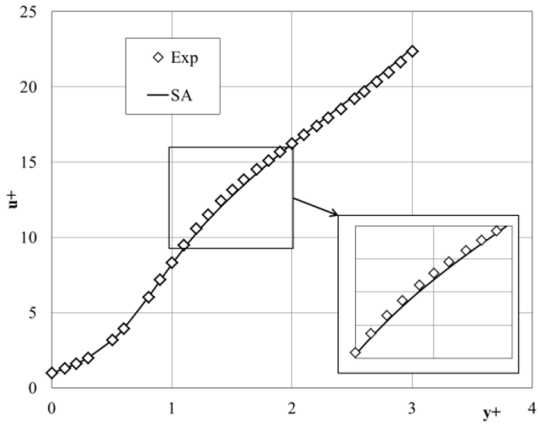

Fig. 8. Transverse distribution of longitudinal velocity.

Numerical studies have shown that the SA model using the McCormack scheme gives results that are closer to the experimental data. [15].

In fig. 9-11 shows the isoline of the dimensionless longitudinal, transverse velocity and Reynolds stress of the flow, respectively.

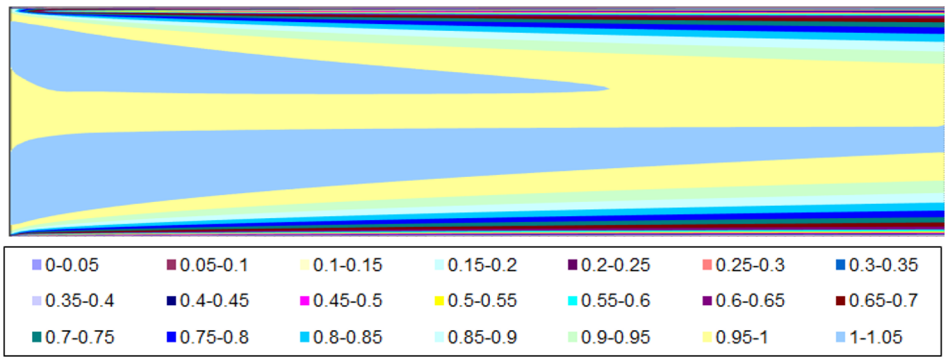

Fig. 9. Isoline of the dimensionless longitudinal flow velocity U/Uref

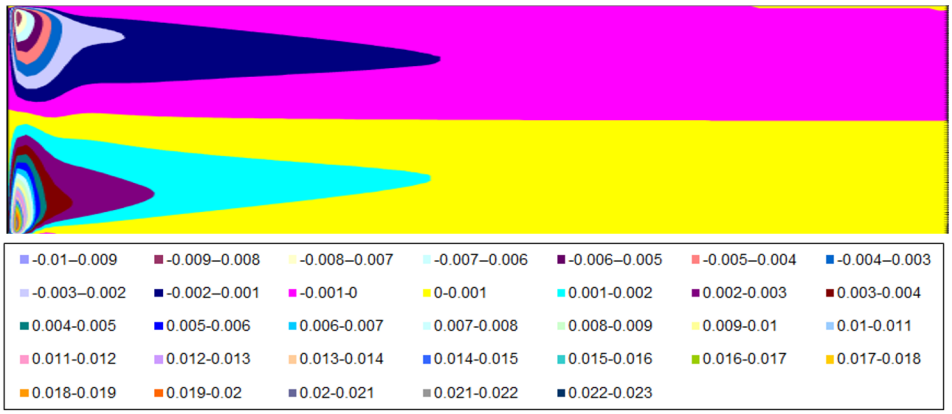

Fig. 10. Isoline of the dimensionless transverse flow velocity V/Uref

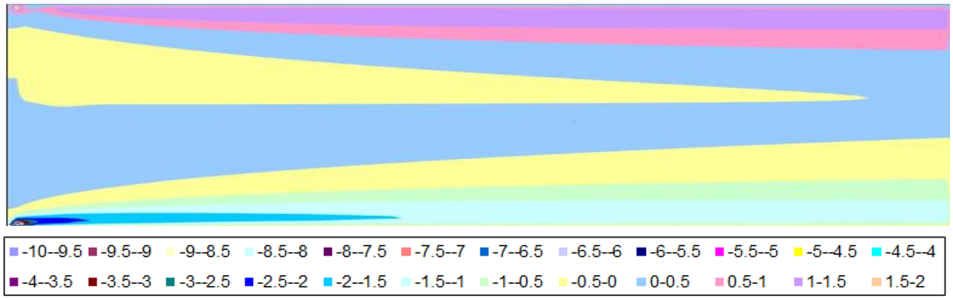

Fig. 11. Isoline of the dimensionless Reynolds Stress $1000\overline{u'v'}/U_{ref}^2$

Figure 12 shows the trajectory of sedimentary fluid with a diameter of 0.01 mm at various Reynolds numbers.

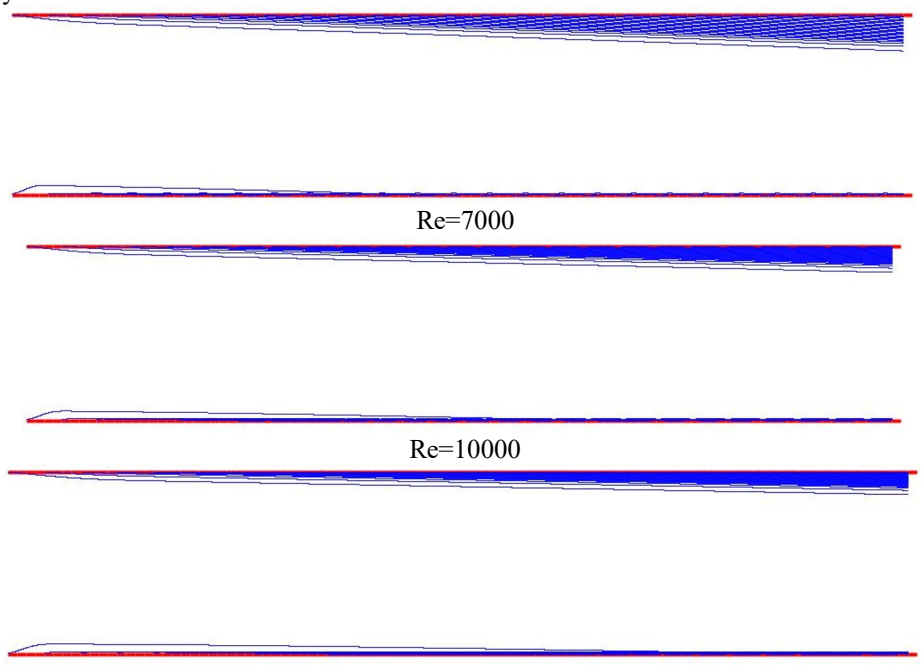

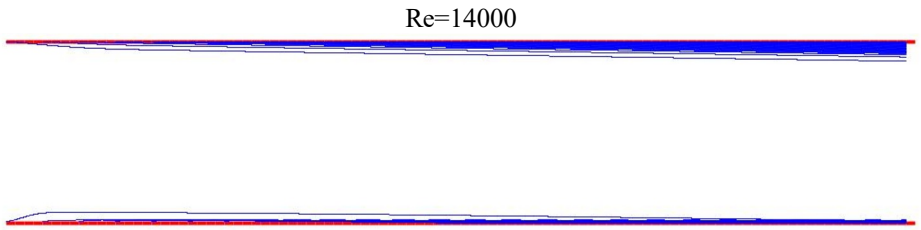

Fig. 12. Trajectory of a sedimentary fluid with a diameter of 0.01 mm at various Reynolds numbers

From figure 12. sedimentary liquid with a diameter of 0.01 mm can be seen at Re=7000 sedimentary liquid remains in the lower part of the channel. At Re=17000 sedimentary fluid is absent from the lower part of the channel.

Figure 13 shows the trajectory of a sedimentary fluid with a diameter of 0.5 mm at various Reynolds numbers.

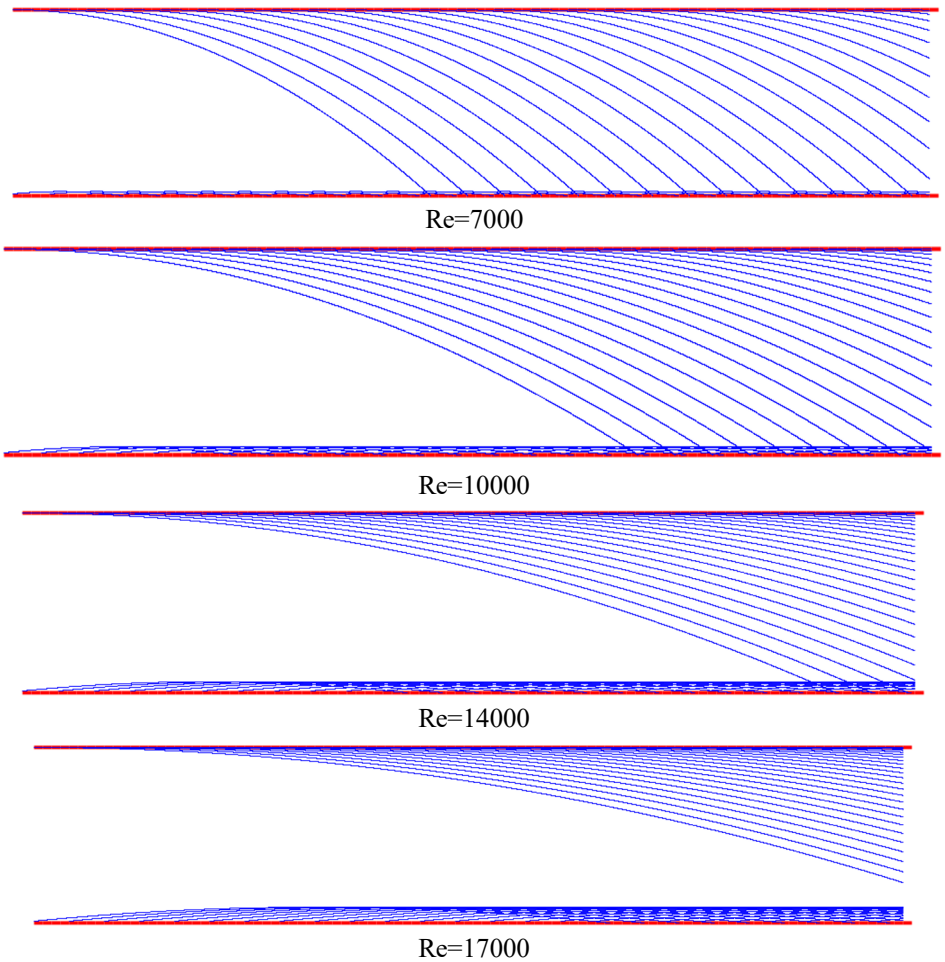

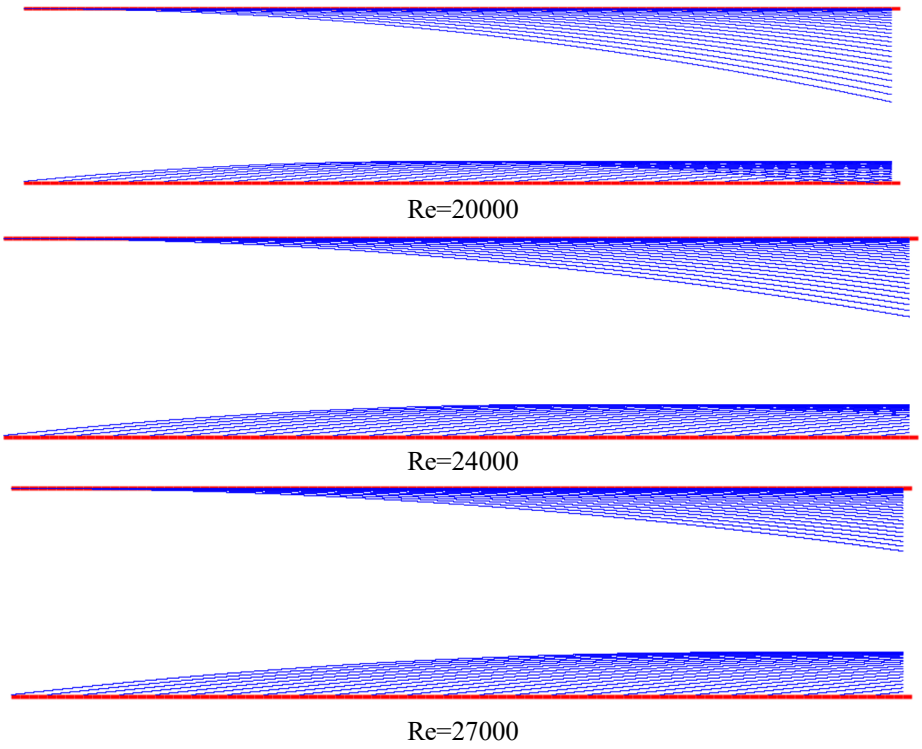

Fig. 13. Trajectory of a sedimentary fluid with a diameter of 0.5 mm at various Reynolds numbers.

Figure 14 shows the trajectory of sedimentary fluid with a diameter of 1 mm at various Reynolds numbers.

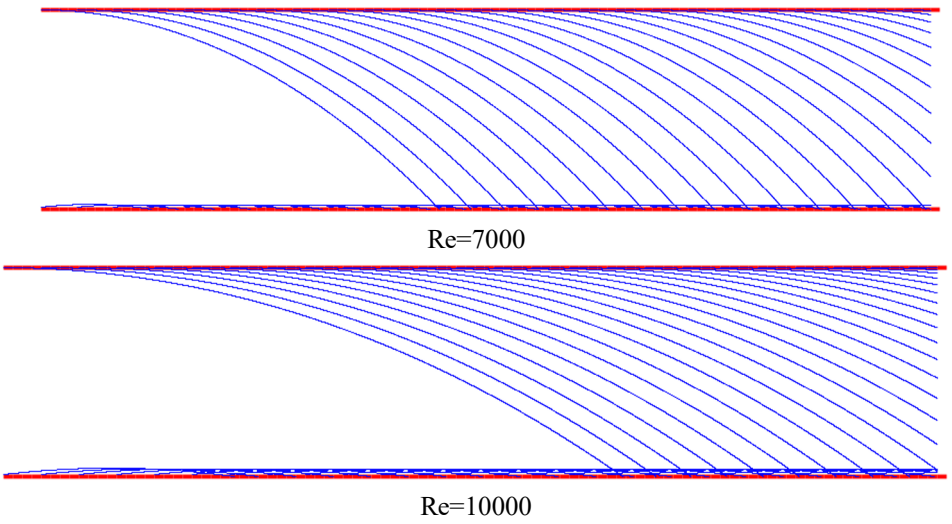

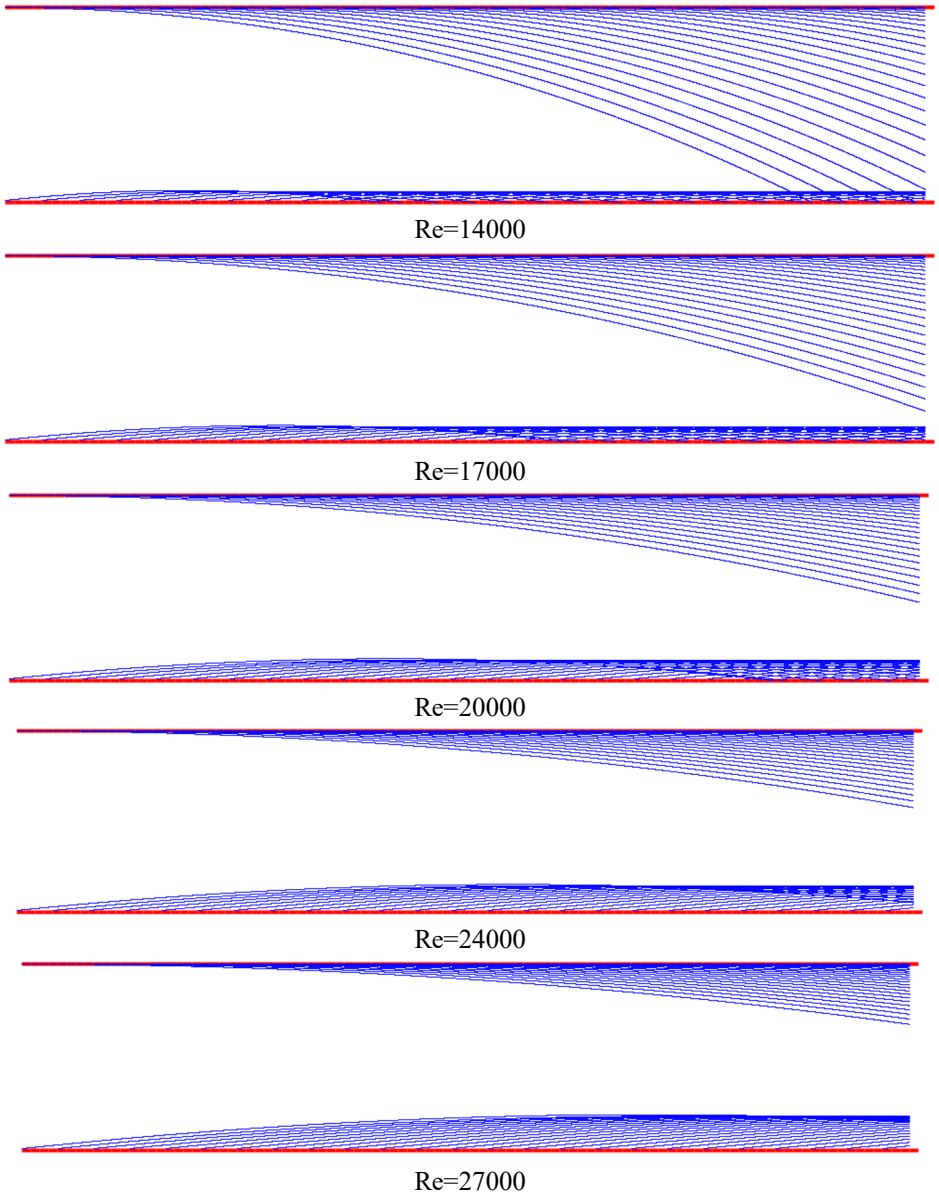

Fig. 14. Trajectory of a sedimentary fluid with a diameter of 1 mm at various Reynolds numbers

In figure 14. it can be seen that it carries away all sedimentary fluid with a diameter of 0.5-1 mm on the lower part of the channel Reynolds number Re>20000 these are values approximately rhubarb U_0=30 м/с.

Figure 15 shows the percentage of residual liquid inside the channel at different Reynolds numbers and diameters.

Re	D=0.01 mm, %	D=0.1 mm, %	D=1 mm, %
7000	44	78	82
10000	36	56	60
14000	18	36	40
17000	2	18	22
20000	0	0.04	0.1
24000	0	0	0
27000	0	0	0

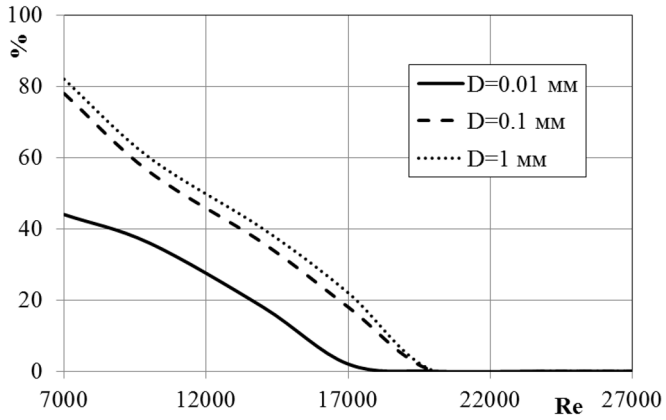

Fig. 15. Percentage of remaining sedimentary fluid inside the channel at different Reynolds numbers and diameters.

8 Conclusion

The paper presents numerical solutions for the flow of a multiphase incompressible viscous fluid in a channel according to the Spalart-Allmares turbulence model. The dependence of the Reynolds number of the momentum loss thickness, the dependence of the friction coefficient on the Reynolds number of the momentum loss thickness, and the transverse distribution of the longitudinal velocity are demonstrated. For the numerical implementation of the turbulence equation, schemes of the second order of accuracy were used. The figures show the Spalart-Allmares model using the McCormack scheme satisfies the experimental results. Moreover, the movement of sedimentary fluid in different diameters and different Reynolds numbers has been studied in the work.

9 Acknowledgments

We take this opportunity to thank all the people who have supported and guided us during the completion of this work.

Conflict of Interest: The authors report no conflicts of interest.

The Source of funding is nil

References

1. V.M. Kovenya, Raznostnie metodi resheniya mnogomernix zadach. Kurs leksiy. (Novosibirskaya Novosib. gos. un-t., 2004)

2. D. Anderson, et.al, Vichislitelnaya gidromexanika i teploobmen: V 2-x t. T. 1: Per. s angl. (Moscow, Mir, 1990)
3. Z.M. Malikov, et.al, Fluid Dynamics **55(8),** 1012-1028 (2020) https://doi.org/10.1134/S0015462820080066
4. E. Son, et.al, Journal of Applied and Computational Mechanics (2020) https://doi.org/10.22055/JACM.2020.31423.1871
5. E. Madaliev et al, E3S Web of Conferences (2021)
6. P.R. Spalart, A. Leonard, *Direct numerical simulation of equilibrium turbulent boundary layers*, in Proc. 5th Symp. on Turbulent Shear Flows, Ithaca (NY, 1985)
7. T. Lund, et.al, Journal of Computational Physics 140, 233–258 (1998)
8. L.G. Loitsyansky, The mechanics of fluid and gas (Moscow, Science, 1987)
9. S.V. Patankar, Numerical Heat Transfer and Fluid Flow (Taylor&Francis, 1980)
10. R.W. MacCormack, AIAA Paper 69—354, Cincinnati Ohie (1969)
11. Z.M. Malikov, Bulletin of Tomsk State University. Mathematics and mechanics **72,** 93-101 (2021)
12. K.E. Schoenherr, Trans. SNAME **40,** 279-313 (1932)
13. D.E. Coles, J. Fluid Mech. **1,** 191–226 (1956)
14. D. Coles, J. Fluid Mech. **1,** 191 (1962)
15. Z.M. Malikov, et.al, Vestnik Moskovskogo gosudarstvennogo texnicheskogo universiteta im. NE Baumana. Seriya Yestestvennые nauki **4,** 24-39 (2021)